ARTICLES

Emission Properties of Manganese-Doped ZnS Nanocrystals

Sameer Sapra,[†] Ankita Prakash,[†] Ajit Ghangrekar,[‡] N. Periasamy,[‡] and D. D. Sarma*[,†,§]

Solid State and Structural Chemistry Unit, Indian Institute of Science, Bangalore 560 012, India, and Department of Chemical Sciences, Tata Institute of Fundamental Research, Mumbai 400 005, India

Received: January 1, 2004; In Final Form: November 4, 2004

We have performed steady-state and time-resolved fluorescence studies on undoped and Mn-doped ZnS nanocrystals with approximately 16 Å diameter. While there is no band-edge emission, the intensity of the steady-state blue fluorescence from ZnS surface states decreases upon Mn incorporation, which gives rise to an orange emission. These results show that Mn incorporation competes very effectively with the donor−acceptor surface states for the energy transfer from the electron−hole pair excited across the band gap. In both undoped and doped samples, the time-resolved fluorescence studies establish the presence of a distribution of decay lifetimes possibly due to a number of emission centers in the nanocrystals. A faster short-time decay of the blue emission in the Mn-doped samples compared to that in the undoped sample suggests an additional decay channel for the surface states via an energy transfer from these states to the dopant levels.

1. Introduction

Doped semiconductors have been studied extensively in the past few decades;[1] recent years have seen a resurgence in the research activity in this field. The interest in doped semiconductors is mainly due to the luminescence properties. One can achieve photoluminescence and electroluminescence at different wavelengths upon doping different ions in the same host semiconductor.[2] The other major application of such doped systems is in the area of magnetism. In this case, the doped magnetic ions are responsible for the magnetic behavior; it can even give rise to half-metallic ferromagnetic systems such as Mn-doped GaAs.[3,4] A new dimension can be added to these magnetically doped semiconductors by controlling the size of the semiconductor particles in the nanometer range. Primarily, $Ga_{1-x}Mn_xAs$,[5] $Zn_{1-x}Mn_xS$ [6−20] and $Cd_{1-x}Mn_xS$ [21−24] have been extensively investigated. Also, other systems such as $Zn_{1-x}Eu_xS$,[25,26] $Zn_{1-x}Cu_xS$,[2] and $Zn_{1-x}Mn_xSe$ [27] have been studied. In doped nanocrystals, the luminescence quantum efficiency is expected to increase as a result of a greater overlap between the electron and the hole of the host semiconductor material with the localized dopant levels. Another advantage is that the band gap of the semiconductor nanocrystals can be tuned between the bulk band gap value and the molecular HOMO−LUMO gap, resulting in a nearly continuous tunability of the band gap over as much as a 2 eV range. This allows tuning of the excitation energy given to the host semiconductor to emit through the dopant levels. Also, it is possible to change the dopant-emission wavelength by changing the size of the nanocrystals as discussed in the case of $Zn_{1-x}Eu_xS$.[26]

Specifically, Mn-doped ZnS is used as a phosphor material for electroluminescent displays.[1] The greater overlap between the host and dopant wave functions in a nanocrystal compared to the bulk material leads to an enhancement in the luminescence intensity due to an enhanced transfer between the host and dopant levels. Furthermore, it has been claimed[8] that the increase in this overlap also leads to a drastic reduction of the radiative lifetime of the Mn orange emission. Subsequent time-dependent fluorescence studies of $Zn_{1-x}Mn_xS$ and $Cd_{1-x}Mn_xS$ nanocrystals have, however, shown that the lifetime of emission through the Mn d levels is hardly affected due to quantum confinement.[13,24] These later studies suggest that the short lifetime of Mn d−d emission reported in ref 8 is in fact an experimental artifact. Recently, it has been shown[19] that the overlap between the semiconductor states and the Mn d levels plays an important role in determining the band gap shifts with the Mn concentration in $Zn_{1-x}Mn_xS$; thus it appears reasonable to expect an effect of doping on the luminescence properties too. To probe the effect of Mn doping on the luminescence properties, we prepared high-quality, nearly monodispersed, $Zn_{1-x}Mn_xS$ samples with different Mn doping concentrations.

2. Methodology

The synthesis procedure is adapted from Nanda et al.[28] who originally used it for the synthesis of undoped ZnS nanocrystals. The $Zn_{1-x}Mn_xS$ nanocrystals were prepared by adding the nominal amounts of $Zn(OAc)_2 \cdot 2H_2O$ and $Mn(OAc)_2 \cdot 4H_2O$ in dimethylformamide along with the capping agent 1-thioglycerol. The sulfides were precipitated upon addition of aqueous sodium sulfide solution slowly. Then the reaction mixture was heated at 100 °C for 12 h. The nanocrystals were precipitated from the clear solution thus obtained by addition of acetone. The nanocrystals were then washed several times with methanol and

* To whom correspondence should be addressed. E-mail: sarma@sscu.iisc.ernet.in.

[†] Indian Institute of Science.

[‡] Tata Institute of Fundamental Research.

[§] Also at Jawaharlal Nehru Centre for Advanced Scientific Research, Bangalore 560 064, India, and the Centre for Condensed Matter Theory, Indian Institute of Science.

10.1021/jp049976e CCC: $30.25
Published on Web 01/14/2005

dried in vacuo for 6 h. The dried powders were used for all the measurements.

X-ray diffraction (XRD) patterns were recorded on a Siemens D5005 diffractometer using Cu Kα radiation. Since the diffracted intensities from these nanocrystals are generally weak, all patterns were recorded at a slow scan rate (10 s/0.1°) in order to get a reasonable signal-to-noise ratio. UV−vis absorption spectra were recorded with powders redissolved in deionized water on a Perkin-Elmer double beam SP8-100 spectrophotometer, and the steady-state fluorescence measurements were carried out with the same solutions on a Shimadzu RF-510 spectrofluorophotometer.

Time-resolved fluorescence measurements were carried out using time-correlated single-photon counting (TCSPC) technique and a high repetition rate picosecond laser source.[29] The nanocrystalline powder sample was taken in a quartz capillary. In some experiments, the sample was dissolved in deionized water and taken in a standard quartz cuvette. The sample was excited by 10 ps, 310 nm laser pulses at a repetition rate of 800 or 400 kHz. The PL from the sample was passed through a cutoff filter (Schott WG 345), a quartz lens, a polarizer oriented at the magic angle (54.7°) with respect to the excitation polarization, and a monochromator. The PL at a selected wavelength was detected at the single-photon level by a microchannel plate photomultiplier (Hamamatsu R2809). In some experiments, the PL decay of "total fluorescence" in the blue emission band (370−520 nm) was obtained by scanning the monochromator (30 nm/min) while detecting photons. The detected photons were time correlated with respect to the excitation laser pulses that are detected by a fast photodiode (IBH, U.K.). The electronic signals from the photodiode and photomultiplier were processed through constant fraction discriminators (CFDs) for generating timing signals, a time-to-amplitude converter (TAC) to generate a voltage pulse that is proportional to the difference in time, and histogrammed in a multichannel analyzer. The instrument response function (IRF) was obtained using a scatterer (MgO powder) instead of the sample. The fwhm of the instrument response function was 40 ps. The detected PL photon rate is less than 0.5% of the excitation rate (i.e. <4000 Hz for an excitation rate of 800 kHz), so that the pile-up error is less than 0.001%. Thus, the slow decay component is better represented in the histogram.

The PL decays were fitted to a multiexponential function (up to five exponentials) by a standard method.[30,31] The method uses iterative reconvolution of IRF and a multiexponential function; lifetime and amplitude parameters were adjusted in successive iterations using the Levenberg−Marquardt algorithm.[32] The average lifetime is defined as $\tau_{av} = \Sigma\alpha_i\tau_i/\Sigma\alpha_i$, where α_i is the amplitude and τ_i is the lifetime. τ_{av} is proportional to the area under the decay curve, and hence τ_{av} is proportional to the quantum yield or steady-state intensity. The goodness criteria of the fit of experimental data are the randomness of weighted residuals, the randomness of autocorrelation function values, and the χ^2 value.[29] PL decays were also fitted using the maximum entropy method (MEM) to obtain a distribution of lifetimes. Details of the MEM are described elsewhere.[33]

3. Results and Discussions

Figure 1 shows the wide-angle X-ray diffraction patterns of undoped and 6% Mn-doped ZnS nanocrystals, as a representative case of the doped samples with all other doped samples exhibiting very similar XRD patterns. The almost identical XRD patterns from the doped and the undoped samples suggest the same structure and size for all the samples. The XRD pattern

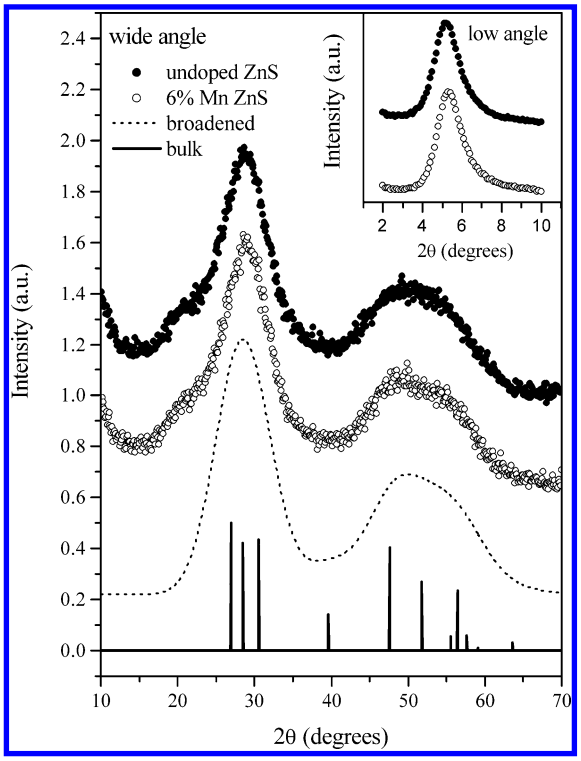

Figure 1. Low-angle and wide-angle X-ray diffraction patterns for the Mn-doped ZnS nanocrystals and bulk wurtzite ZnS.

from the JCPDS-ICDD database for bulk ZnS crystallizing in the wurtzite structure is also shown in the same figure by the bar diagram. The wide-angle XRD pattern for the bulk system exhibits several peaks in the range of $2\theta = 20-65°$, characteristic of the wurtzite structure. Over the same range, the XRD patterns from the nanocrystal samples exhibit two broad peaks. It is well-known that the XRD pattern from the nanocrystal broadens due to the finite size effect, which is described in terms of the Scherrer formula,

$$L = \frac{0.9\lambda}{B\cos\theta} \tag{1}$$

Here, the coherence length, L, is related to the full width at half-maximum (fwhm), B, of the peak centered at θ, recorded with X-rays of wavelength, λ. The diameter, d, of the nanocrystal is then given by $d = (4/3)L$, assuming the particles are spherical in shape. To estimate the size of the nanocrystals from the broadening of the XRD pattern, we convolute the entire XRD pattern of bulk ZnS with a Gaussian function whose width depends on the size of the nanocrystal and the angle of diffraction, according to the Scherrer formula. This gives the simulated pattern from nanocrystals for any given size. We systematically change the estimate of the nanocrystal size within a least-squared-error approach such that the simulated pattern agrees best with the experimentally observed one over the entire range of angles. We find that the choice of 16 Å for the nanocrystal diameter provides the best description, illustrated by the good agreement between the experimental data and the simulated XRD (dashed line) for a 16 Å nanocrystal with the wurtzite structures in Figure 1. The size is further confirmed by the low-angle X-ray diffraction, exhibiting a peak at 5.2°, as shown in the inset. Using Bragg's Law, this gives an estimate of the particle size to be 17 Å for both the doped and the undoped samples. This establishes that we have been able to synthesize fixed-size Mn-doped ZnS nanocrystals with varying Mn concentration.

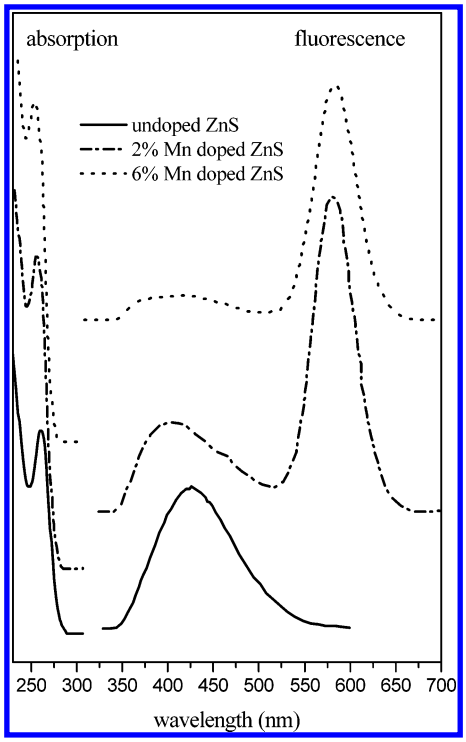

Figure 2. UV−vis absorption and fluorescence emission spectra for undoped and Mn-doped ZnS nanocrystals. Note that the spectra are normalized and shifted for clarity.

We show the basic characterization of these nanocrystal samples in terms of UV−visible absorption spectra and fluorescence spectra in Figure 2. First we discuss the absorption results, shown on the left side in Figure 2. The UV−vis absorption spectra show sharp absorption edges and sharp excitonic features characteristic of nearly monodispersed nanocrystals in every case. The UV-absorption edge provides us a reliable estimate of the band gap of any system. From the absorption edge (∼260 nm) of the undoped ZnS nanocrystals, we obtain a band gap of 4.77 eV. The bulk band gap of ZnS is 3.67 eV. This implies that the band gap increases by 1.1 eV in the nanocrystal sample. To correlate the size of the nanocrystals with the band gap shift, one compares the calculated variation of band gap as a function of the size with the experimental values from the UV−vis absorption spectra. We have developed a tight binding model[5,34−37] that consists of the sp^3d^5 orbital basis on both the cation and the anion and includes the cation−anion and the anion−anion interactions. Comparing with the results obtained in these works, we estimate the diameter of the nanocrystals to be ∼16 Å, in very good agreement with the XRD results.

The plots on the right-hand side of Figure 2 show the fluorescence emission spectra for the nanocrystal samples. The spectra have been recorded at an excitation wavelength of 290 nm (4.3 eV). In the undoped ZnS nanocrystals we observe only one single band centered at ∼425 nm. This is clearly at a much longer wavelength (lower energy) than would be expected from a band gap emission process; in fact, we do not observe any band gap emission in the samples reported here. This red-shifted emission appearing in the blue region of the visible spectrum, corresponds to the defect-state recombination; these defect states are mostly on the surface of the nanocrystals. Since we have used an excess of the cations in the synthesis procedure, we expect sulfur vacancies at the surface giving rise to Zn dangling bonds that form shallow donor levels. Thus, the recombination is mainly between these shallow donor levels and the valence band, arising from a very fast energy transfer from the electron−hole pair excited across the band gap of the nanocrystal. Becker et al.[38] reported that S^{2-} vacancies even in bulk ZnS lead to emission at 428 nm. Upon Mn addition in the nanocrystal samples, an orange emission band develops at ∼580 nm, corresponding to the well-known $^4T_1-^6A_1$ Mn d−d transition. Similar results have been reported recently[19] in the case of considerably larger (∼24 Å) Mn-doped ZnS nanocrystals, though the relative orange emission appears to be considerably higher in the present case for comparable levels of doping. Thus, the emission spectrum of the 6% Mn-doped sample in the present study is entirely dominated by the Mn orange emission. Noting that the excitation process generates an electron−hole pair across the band gap (4.77 eV) of the ZnS nanocrystal host, the present results make it evident that there is a more efficient energy transfer of the excitation from the host to the doped Mn site compared to that of the defect states in these materials; this suggests a strong coupling between the Mn d levels and the host states. The energy transfer is unlikely to occur directly from the semiconductor band states to the low-lying Mn d states. The transfer is most probably to the higher lying Mn states that are closer in energy to the ZnS conduction band, as has been discussed by Tanaka.[39] In principle, the faster transfer of the excitation to the Mn may also be facilitated by a much faster decay rate at the dopant sites, as originally suggested;[8] therefore, we have investigated the decay time scales of various features in the fluorescence spectra of these samples.

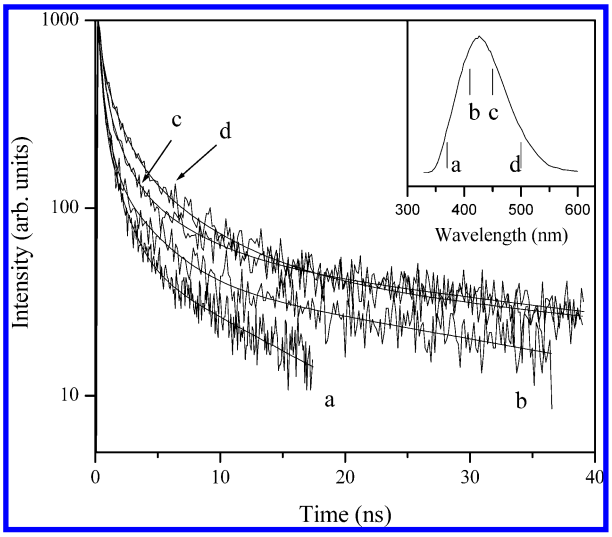

Figure 3. PL decays of undoped sample at different emission wavelengths: (a) 370, (b) 410, (c) 450, and (d) 500 nm. The PL decays are normalized to a constant peak intensity of 1000.

The PL decay of undoped ZnS nanocrystals consisted of fast and slow decay components. The PL decay was therefore obtained at high (39 picosec/channel) and low (3.9 nanosec/channel) resolutions to capture more accurately the fast and slow components, respectively. The variation of the PL decay at different emission wavelengths within the blue emission band of the undoped ZnS sample centered at 425 nm was studied. The PL decay was not identical at all emission wavelengths, exhibiting some systematic variations. Figure 3 shows the variation at four different wavelengths for the undoped sample in the high-resolution mode. The relative fraction of the short decay component decreased with an increasing wavelength, as is evident from the figure. These results confirm the heterogeneous character of emission centers in the undoped sample. Also, it has been recently suggested, by performing single quantum-dot fluorescence decay studies, that the same emission center

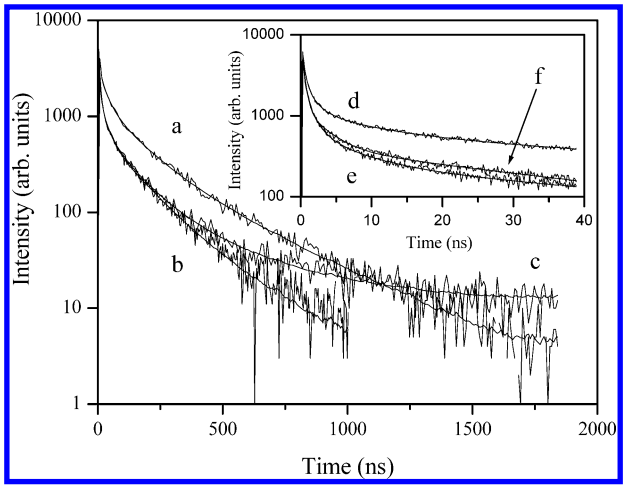

Figure 4. PL decay at 445 nm for undoped (a and d), 2% Mn-doped (b and e), and 6% Mn-doped (c and f) ZnS nanocrystals. The PL decays a−c are obtained at low resolution (3.9 ns/ch), and d−f are obtained at high resolution (0.039 ns/ch). The PL decays were best fitted (χ^2 value less than 1.1) to a five-exponential function, and the smooth lines through the noisy data are the calculated values.

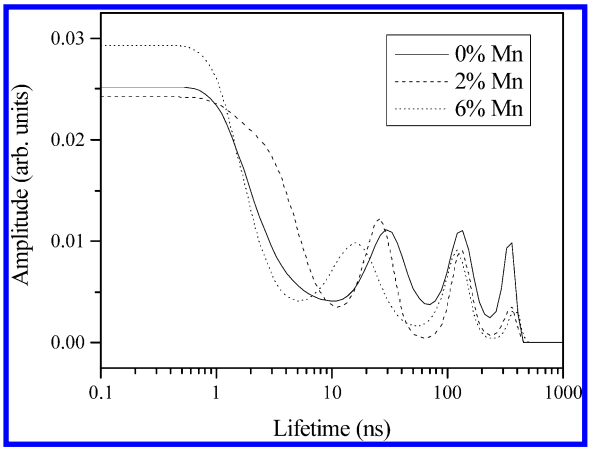

Figure 5. Distribution of lifetimes obtained by MEM for the PL decay at 445 nm for undoped (solid line), 2% Mn-doped (dashed line), and 6% Mn-doped (dotted line) samples which are shown in Figure 4a−c. The χ^2 value is ∼1 for the distribution. The distribution for the undoped sample has peaks at ∼30, 140, and 360 ns and unstructured below 10 ns. The distribution for the Mn-doped sample is similar except for reduced amplitudes for lifetimes longer than 10 ns. The amplitudes are normalized so that the sum is unity.

exhibits different decay times.[40] The above results indicate that the nature of the excited states and the radiative/nonradiative mechanisms in undoped ZnS nanocrystals are considerably complex, some aspects of which are discussed below.

The decay plot a in the mainframe and d in the inset of Figure 4 show the time-resolved luminescence decay at the peak (445 nm) of the blue emission band of undoped ZnS nanocrystals at low and high resolutions, respectively. The decay at low or high resolution is evidently not monoexponential and required a multiexponential function for a satisfactory fit, shown by the solid smooth line through the data. The PL decays at 445 nm for the 2% (curves b and e) and 6% Mn-doped (curves c and f) samples are also shown in Figure 4. A direct comparison of the decay in the doped samples can be made with that of the undoped sample, since the peak intensities are normalized in every case. Mn doping results in a drastic reduction of luminescence quantum yield, proportional to the area under the decay curve, of the 370−520 nm emission from ZnS nanocrystals even for a small amount of Mn doping.

The method of preparation of ZnS nanocrystals allows the possibility that a fraction of the nanocrystals may not have a single Mn ion. This fraction can be estimated as follows. With the assumption that the nanocrystals are all of uniform size (diameter, 16 Å), justified by sharp excitonic peaks in the absorption spectra indicating a very narrow size distribution, and that the unit cell volume is the same as that of bulk crystal, supported by XRD results, there are ∼75 Zn ions per nanocrystal. Mn dopings at 2 and 6% levels imply that there are, on the average, 1.5 and 4.5 Mn ions/nanocrystal, respectively. A random distribution of Mn ions would obey Poisson statistics. The probability for n Mn centers in a nanocrystal is given as,

$$P(n) = \frac{x^n e^{-x}}{n!} \qquad (2)$$

where x is the mean number of Mn centers per nanocrystal. The probability, $P(0)$, that a nanocrystal has zero Mn center is thus e^{-x}, yielding $P(0) = 0.22$ for 2% doping. If we assume that the presence of a Mn center in a nanocrystal leads to complete energy transfer from the band gap excitation to the Mn states without any energy transfer to the defect states, we would expect a 78% reduction in the blue emission in the 2% Mn-doped sample. A similar analysis for 6% Mn-doped ZnS suggests a 99% reduction in the blue emission. Thus, the ratio of the emission $(\text{blue/orange})_{6\%}$ to $(\text{blue/orange})_{2\%}$, calculated using eq 2, is $(1/99) \times (78/22) = 0.036$, whereas the same ratio obtained from the experimental fluorescence data (Figure 2) is 0.49. If we assume that the direct excitation of Mn ion is negligible at 290 nm, the substantially higher value (0.49) of the experimental ratio indicates that energy transfer from the conduction band to the Mn ion is not complete in a nanocrystal containing an Mn ion. That is, defect states that lead to blue emission are operative even in these Mn-containing nanocrystals. This raises an interesting question that if the excited defect states and Mn ion coexist in the same nanocrystal, could there be energy transfer from the defect state to the Mn ion. Evidence for this is presented in the analysis of PL decays of blue emission discussed below.

The above results indicate the growth of the orange emission intensity at the cost of the blue emission with increasing concentration of Mn, as primarily driven by a very efficient energy transfer between the host and the impurity separated by a few angstroms in the nanocrystals, competing with the energy-transfer process from the band states to the defect, primarily surface, states. In this context, it is important to note that the Mn-doped samples consistently exhibit a more rapid decay of 445 nm blue PL intensity (curves c and f) in the short time domain compared to the undoped sample (curve d). Since PL intensity at the blue emission at any given time after the initial excitation is proportional to the number of excited defect states, a more rapid decay in this PL intensity with time in the presence of Mn in the sample must imply that some of the excited defect states de-excite without the blue emission, most probably via a nonradiative energy transfer to the Mn states.

It is to be noted that the decays beyond 20−30 ns appear similar for all the samples irrespective of Mn doping. To obtain a quantitative comparison, the PL decays of undoped and Mn-doped samples were fitted to a distribution of lifetimes (0.1−1000 ns) by the maximum entropy method. Figure 5 shows the distribution of lifetimes for undoped and Mn-doped samples which fit the PL decays shown in Figure 4 (a−c). Each of the three distributions is found to be broad and unstructured for $t < 5$ ns with three distinct peaks in the higher time domain. While the physical origins of these three peaks are not clear to

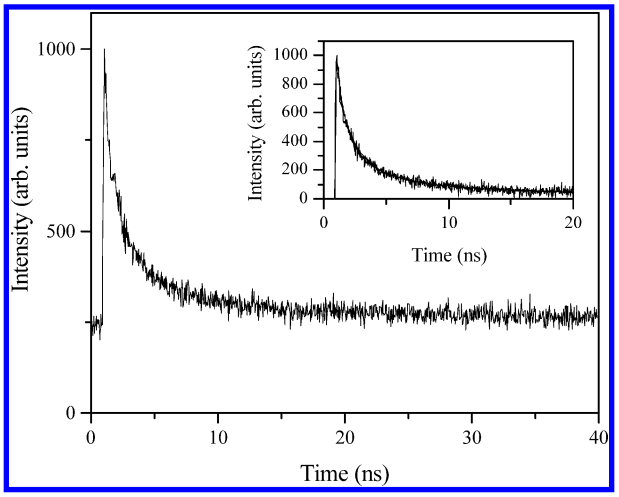

Figure 6. PL decay of the 2% Mn-doped sample at 580 nm. The fast (nanosecond) decay component is seen on top of the background-like (~240 counts), long-lifetime emission of Mn^{2+}. The inset shows the overlap of the fast component of the Mn-doped sample and the PL decay of of the undoped sample at 580 nm. The peaks are normalized to 1000 in both cases. For the undoped case, the background is zero, whereas it is ~240 counts in the doped sample. This is subtracted to obtain a zero background as shown in the inset.

us, it is important to note that these results quantitatively support the idea of an energy transfer from the defect states to the Mn states in terms of a systematic shift of the first peak toward a lower time domain with increasing Mn concentration. The longer time decay of blue PL intensity is seen to be essentially insensitive to Mn doping.

Figure 6 shows the PL decay at 580 nm for the undoped and Mn-doped samples. The PL decay of the undoped sample is similar to the decays at other emission wavelengths (Figure 3); as in this case, the finite intensity at 580 nm is obviously due to the tail of the low-energy surface states of ZnS. The PL decay of the Mn-doped sample at 580 nm consists of a fast component and an extremely slow component. The extremely slow component appears like the background in the TCSPC experiment because the interval between two excitation pulses is 25 μs, which is much shorter than the characteristic time scale of the slow decay component. It is important to note here that the decay time of Mn^{2+} emission in bulk $Zn_{1-x}Mn_xS$ is 1.9 ms.[13] In this study, we compared the fast component of the PL decay at 580 nm of the Mn-doped sample with that of the undoped sample by overlapping the two in the inset to Figure 6, thereby establishing that the fast decay of Mn-doped samples is identical to that of the undoped sample. Hence, we conclude that the fast decay at 580 nm in Mn-doped samples is due to the overlapping tail of the PL from surface states of ZnS and not due to Mn^{2+}.

The photophysics of the undoped and Mn-doped nanocrystals may be explained using the schematic diagram (Figure 7). In undoped crystals, the blue emission arises from the de-excitation of defect states following the energy transfer from the excitation, as shown. In Mn-doped crystals, both blue (weak) and orange (strong) emissions are observed and the dominant orange emission is due to Mn ion. Our results suggest that the excited Mn states, responsible for the orange emission, are primarily formed by an energy transfer from the electron−hole pair excited across the band gap to the Mn d states, consistent with previous reports.[14] However, a definite contribution to the orange emission by the energy transfer from the defect states is also indicated by the faster decay of the defect-state emission in the doped samples in Figure 4. Also, the MEM results shown in

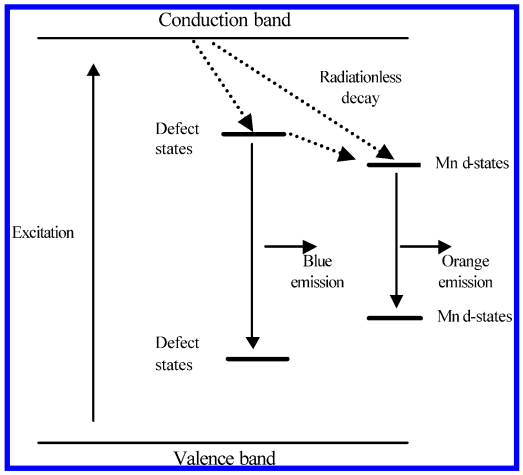

Figure 7. Schematic for the decay of electrons via different channels in Mn-doped ZnS nanocrystals.

Figure 6 support this idea. There are three lifetime peaks at 30, 140, and 360 ns for the blue emission of the undoped sample. A short-range Dexter-type mechanism of energy transfer from defect states to Mn ions, assuming that an acceptor level of the Mn ion lies close to the defect excited state, would indicate a decrease in the lifetime of the defect state. Such a systematic reduction in lifetime is indeed observed for the 30 ns peak, though not for other lifetime peaks.

4. Conclusions

We have studied the steady-state fluorescence and time-resolved photoluminescence of undoped and Mn-doped ZnS nanocrystals with a fixed diameter. We find that the intensity of the blue emission arising due to the defect states of the nanocrystals gets diminished upon Mn doping; the host semiconductor transfers the energy to the Mn d states in preference to the donor−acceptor surface states, which then de-excite to give an orange emission. Time-resolved PL measurements show that the blue component decays at a very fast rate (on the order of nanoseconds) compared to the orange emission (about a few milliseconds). The fast component in the orange emission that led researchers to believe initially that the Mn emission rates are enhanced in ZnS nanocrystals compared to the bulk, actually belongs to the tail of the surface/defect state emission. The excitation pathway for the dopant site is shown to have two contributions, namely, the energy transfers directly from the host to the Mn d states and another via an energy transfer from the defect sites to the Mn d levels.

Acknowledgment. We thank Prof. A. K. Sood for useful discussion and the Department of Science and Technology for funding this project.

References and Notes

(1) Furdyna, J. K. *J. Appl. Phys.* **1988**, *64*, R29.
(2) Xu, S. J.; Chua, S. J.; Liu, B.; Gan, L. M.; Chew, C. H.; Xu, G. Q. *Appl. Phys. Lett.* **1998**, *73*, 478.
(3) Ohno, H. *Science* **1998**, *281*, 951.
(4) Ohno, H. *J. Magn. Magn. Mater.* **1999**, *200*, 110.
(5) Sapra, S.; Sarma, D. D.; Sanvito, S.; Hill, N. A. *Nano Lett.* **2002**, *2*, 605.
(6) Wang, Y.; Herron, N.; Moller, K.; Bein, T. *Solid State Commun.* **1991** *77*, 33.
(7) Khosravi, A. A.; Kundu, M.; Kuruvilla, B. A.; Shekhawat, G. S.; Gupta, R. P.; Sharma, A. K.; Vyas, P. D.; Kulkarni, S. K. *Appl. Phys. Lett.* **1995**, *67*, 2506.

(8) Bhargava, R. N.; Gallagher, D.; Hong, X.; Nurmikko, A. *Phys. Rev. Lett.* **1994**, *72*, 416.
(9) Soo, Y. L.; Ming, Z. H.; Huang, S. W.; Kao, Y. H.; Bhargava, R. N.; Gallagher, D. *Phys. Rev. B* **1994**, *50*, 7602.
(10) Murase, N.; Jagannathan, R.; Kanematsu, Y.; Watanabe, M.; Kurita, A.; Hirata, K.; Yazawa, T.; Kushida, T. *J. Phys. Chem. B* **1999**, *103*, 754.
(11) Sooklal, K.; Cullum, B. S.; Angel, S. M.; Murphy, C. J. *J. Phys. Chem. B* **1996**, *100*, 4551.
(12) Chen, W.; Sammynaiken, R.; Huang, Y.; Malm, J.-O.; Wallenberg, R.; Bovin, J.-O.; Zwiller, V.; Kotov, N. A. *J. Appl. Phys.* **2001**, *89*, 1120.
(13) Bol, A. A.; Meijerink, A. *Phys. Rev. B* **1998**, *58*, R15997.
(14) Chen, W.; Sammynaiken, R.; Huang, Y. *J. Appl. Phys.* **2000**, *88*, 5188.
(15) Chen, W.; Su, F.; Li, G.; Joly, A. G.; Malm, J.-O.; Bovin, J.-O. *J. Appl. Phys.* **2002**, *92*, 1950.
(16) Smith, B. A.; Zhang, J. Z.; Joly, A.; Liu, J. *Phys. Rev. B* **2000**, *62*, 2021.
(17) Chen, W.; Joly, A. G.; Zhang, J. Z. *Phys. Rev. B* **2001**, *64*, 041202**R**.
(18) Tanaka, M.; Masumoto, Y. *Chem. Phys. Lett.* **2000**, *324*, 249.
(19) Sapra, S.; Nanda, J.; Anand, A.; Bhat, S. V.; Sarma, D. D. *J. Nanosci. Nanotechnol.* **2003**, *3*, 392.
(20) Su, F. H.; Ma, B. S.; Fang, Z. L.; Ding, K.; Li, G. H.; Chen, W. *J. Phys.: Condens. Matter* **2002**, *14*, 12657.
(21) Counio, G.; Gacoin, T.; Boilot, J. P. *J. Phys. Chem. B* **1998**, *102*, 5257.
(22) Feltin, N.; Levy, L.; Ingert, D.; Pileni, M. P. *J. Phys. Chem. B* **1999**, *103*, 4.
(23) Levy, L.; Hochepied, J. F.; Pileni, M. P. *J. Phys. Chem.* **1996**, *100*, 18322.
(24) Chamarro, M. A.; Voliotis, V.; Grousson, R.; Lavallard, P.; Gacoin, T.; Counio, G.; Boilot, J. P.; Cases, R. *J. Cryst. Growth* **1996**, *159*, 853.
(25) Chen, W.; Malm, J.-O.; Zwiller, V.; Huang, Y.; Liu, S.; Wallenberg, R.; Bovin, J.-O.; Samuelson, L. *Phys. Rev. B* **2000**, *61*, 11021.
(26) Chen, W.; Malm, J.-O.; Zwiller, V.; Wallenberg, R.; Bovin, J.-O. *J. Appl. Phys.* **2001**, *89*, 2671.
(27) Norris, D. J.; Yao, N.; Charnock, F. T.; Kennedy, T. A. *Nano Lett.* **2001**, *1*, 3.
(28) Nanda, J.; Sapra, S.; Sarma, D. D.; Chandrasekharan, N.; Hodes, G. *Chem. Mater.* **2000**, *12*, 1018.
(29) O'Connor, D. V.; Phillips, D. *Time Correlated Single Photon Counting*; Academic Press: London, 1984.
(30) Periasamy, N.; Doraiswamy, S.; Maiya, B. G.; Venkataraman, B. *J. Chem. Phys.* **1988**, *88*, 1638.
(31) Periasamy, N. *Biophys. J.* **1988**, *54*, 961.
(32) Press, W. H.; Flannery, B. P.; Teukolsky, S. A.; Vetterling, W. H. *Numerical Recipes in C*, 2nd ed.; Cambridge University Press: Cambridge, U.K., 1992; p 683.
(33) Swaminathan, R.; Periasamy, N. *Proc. Ind. Acad. Sci.* **1996**, *108*, 39.
(34) Sapra, S.; Shanthi, N.; Sarma, D. D. *Phys. Rev. B* **2002**, *66*, 205202.
(35) Sapra, S.; Sarma, D. D. *Phys. Rev. B* **2004**, *69*, 125304.
(36) Sapra, S.; Viswanatha, R.; Sarma, D. D. *J. Phys. D: Appl. Phys.* **2003**, *36*, 1595.
(37) Viswanatha, R.; Sapra, S.; Satpati, B.; Satyam, P. V.; Dev, B. N.; Sarma, D. D. *J. Mater. Chem.* **2004**, *14*, 661.
(38) Becker, W. G.; Bard, A. J. *J. Phys. Chem.* **1983**, *87*, 4888.
(39) Tanaka, M. *J. Lumin.* **2002**, *100*, 163.
(40) Fisher, B. R.; Eisler, H. J.; Stott, N. E.; Bawendi, M. G. *J. Phys. Chem. B* **2004**, *108*, 143.